scientific reports

Check for updates

OPEN

Broadband slant-polarized series-fed microstrip patch antenna array based on magnetic current feeding technology

Yue Zhao[1,2,3,4], Xinran Ji[1,2,3,4], Binyi Ma[1,2,3,4], Yuheng Si[1,2,3,4], Yilin Jia[2,3,4,6], Qiannan Wu[2,3,4,6]✉ & Mengwei Li[1,2,3,4,5]✉

This paper introduces a broadband 45° slant dual-polarized series-fed microstrip patch antenna array with low VSWR, based on magnetic current feeding technology. Conductive strips connect the radiating elements, minimizing out-of-phase currents to improve broadside directivity. A ring resonator is introduced by slotting the microstrip line, adding new resonant frequency bands, while the feed network design enables the formation of radiation modes similar to a magnetic current-fed array. The series-fed array's wide bandwidth is achieved by combining the fundamental mode of side-shorted microstrip patch antennas with additional modes from the feed structure. A fabricated three-element linear array with central feeding demonstrated an impedance bandwidth of 3–6 GHz (67%) and a minimumVSWR of 1.007, offering simple feeding and low loss. This design is well-suited for applications requiring high directivity and dual polarization, such as 5G communication, drones, radar systems, satellite communications, and IoT networks.

Keywords Multiple-Input, Multiple-Output (MIMO), Magnetic current, Series-fed antenna array, Low voltage standing wave ratio (VSWR), Broadband

MICROSTRIP patch antennas (MPA) are widely utilized in wireless communication systems due to their simple structure, low manufacturing cost, ease of integration, and compact size. However, despite their excellent performance in many applications, several pressing issues still need to be addressed. Firstly, microstrip patch antennas typically have a narrow bandwidth, limiting their use in broadband communications, especially when handling multiple signal bands is required, making them less flexible. Secondly, in dense antenna arrays, microstrip patch antennas are prone to mutual coupling effects, which can lead to reduced communication capacity and increased signal interference, thereby degrading the overall system performance. Furthermore, traditional microstrip patch antennas usually have a single polarization, which fails to meet the diverse polarization requirements of modern communication systems in complex environments. Consequently, to enhance the performance of microstrip patch antennas, researchers have recently focused on increasing bandwidth, reducing mutual coupling effects, and achieving multi-polarization through extensive research and optimization efforts[1,2].

To meet the high gain requirements of line-of-sight communication scenarios, such as satellite communications, base stations, and outdoor customer equipment, researchers have proposed various techniques to enhance antenna directivity. Among these, array antennas are a conventional method widely used to increase antenna gain. Based on different feeding methods, array antennas can be categorized into series-fed arrays and parallel-fed arrays. Comparatively, series-fed antenna arrays have advantages such as a simple feed network structure, low insertion loss, and compact size. However, series-fed arrays typically exhibit a narrow operational bandwidth. This is due to Series-fed arrays often exhibit narrow operational bandwidth characteristics, primarily due to the intrinsic nature of signal propagation in a linear array configuration. When using a common feed line, the input signal must traverse multiple antenna elements in sequence, with each transition introducing

[1]School of Instrument and Electronics, North University of China, Taiyuan 030051, China. [2]School of Instrument and intelligent future technology, North University of China, Taiyuan 030051, China. [3]Academy for Advanced Interdisciplinary Research, North University of China, Taiyuan 030051, China. [4]Center for Microsystem Intergration, North University of China, Taiyuan 030051, China. [5]Key Laboratory of Dynamic Measurement Technology, North University of China, Taiyuan 030051, China. [6]School of Semiconductors and Physics, North University of China, Taiyuan 030051, China. ✉email: qiannanwoo@nuc.edu.cn; lmwprew@163.com

cumulative transmission loss and signal uncertainties due to multiple reflections and transmission processes. These factors lead to phase variations and amplitude distortions, effectively limiting the achievable bandwidth. The common feed line also exacerbates signal phase differences across elements, resulting in destructive interference over wider frequency ranges and thus reducing the overall bandwidth[3]. Consequently, series-fed arrays often display narrow bandwidth characteristics[4,5]. Moreover, due to the complexity of the array structure and interactions among elements, the Voltage Standing Wave Ratio (VSWR) can be significantly affected. In recent years, various series-fed MPA have been reported, with relative bandwidths of 1.34%[6], 1.39%[7], 0.087%[5], and 5.7%[8], all of which achieve relatively narrow operational bandwidths. Additionally, other types of microstrip patch antennas have been extensively studied and reported, including slot-fed arrays[9–13], dual-polarized antenna arrays[14–18], and slot arrays[19,20]. However, these antennas also generally have operational bandwidths of less than 10%, and the impedance matching often results in poor VSWR, potentially causing power dissipation in the system. Although performance can be improved through optimization techniques such as matching stubs, these methods also increase system complexity and hardware costs. In large scale Multiple-Input Multiple-Output (MIMO) base stations, the system typically consists of multiple sub-arrays, each containing three or four patch elements, which are fed through a corporate feed network[21–23]. The use of numerous power dividers in large scale MIMO feed networks not only increases dissipation loss but also elevates hardware costs. In contrast, series-fed antenna arrays, by avoiding the use of power dividers, offer the advantages of simpler structure and higher efficiency.

In engineering applications and relevant literature, broadband antenna arrays based on microstrip line structures have been widely reported[9–32]. However, research on broadband series-fed antenna arrays is relatively limited. Among the few existing studies, such as[33–35] a low sidelobe end fed 45° polarized microstrip comb linear array has been proposed. This antenna array demonstrates excellent impedance bandwidth, but its good radiation performance is confined to a narrow bandwidth range. Furthermore, this design requires an air gap between the substrates, which increases the complexity of antenna fabrication. Another study[36] introduced a broadband center-fed series patch antenna array, achieving a bandwidth of 26.1%. However, it has only a single polarization direction.In the current body of research, series-fed arrays with slant polarization are exceedingly rare. Therefore, designing a series-fed array that not only offers a wide bandwidth and good radiation performance but also excels in impedance matching remains a significant challenge.

Based on the aforementioned studies, this paper proposes an ultra wideband, low VSWR, dual-polarized three-element series-fed slant-polarized MPA array. This design offers the advantages of simplicity and low cost. The antenna array utilizes magnetic current feeding and incorporates ring resonators and slot structures as resonant elements. By employing a dual-radiator design with a two-layer main structure, the array achieves a wide bandwidth and a low VSWR. The impedance bandwidth of this antenna array ranges from 3 GHz to 6 GHz (67%), with a VSWR of 1.0074 and a maximum gain of 14 dBi. This structure can be widely applied in various fields such as 5G communication systems, drones, radar systems, satellite communications, and IoT networks.

Working principle

Sides-Shorted MPA

Due to the short-circuited structure of the ring resonators at both ends of the antenna, the TM_{11} mode is effectively suppressed, allowing the TM_{21} mode to be excited as the fundamental mode in the side-shorted MPA(SSMPA). Similar to the TM_{11} mode, the magnetic field of the TM_{21} mode exhibits an in-phase distribution along the horizontal direction and can be excited through coupling slots. In fact, the traditional microstrip slot feeding method can be regarded as a current excitation method, and the microstrip line current (Je) on the slot can induce a ring H-field pattern around the slot, which introduces a horizontal H-field to excite the TM21 mode in SSMPA. At the same time, the magnetic current (Jm) along the coupling slot can also generate a horizontal H-field within the antenna cavity. Therefore, the TM21 mode of the antenna structure transmission surface can be driven by two types of excitation along the slot, i.e., current excitation and magnetic current excitation. By introducing magnetic current into the opening or gap of the microstrip antenna, the magnetic current in the gap is able to form a horizontal magnetic field component in the antenna cavity or other radiating surface and resonate with a specific mode of the antenna, such as TM mode, further enhancing the radiation characteristics. This dual excitation mechanism not only increases the flexibility of the antenna's mode excitation, but also optimizes its radiation characteristics and bandwidth to achieve more efficient energy transfer, as illustrated in Fig. 1.

Magnetic-Current-Fed MPA element

To validate the concept of magnetic current excitation, a magnetic current-fed side-shorted microstrip patch antenna (SSMPA) element was designed, as shown in Fig. 2(a). According to "Love's equivalence principle"[27], an equivalent magnetic current is obtained along the quasi-magnetic wall at the open side of the divided cavity. Based on this, a microstrip-fed quarter-mode cavity (QMC) was designed as the magnetic current feeding structure, positioned on the top layer. The ring resonators are deposited on a substrate. These rings are strongly coupled by a distributed capacitance, which is formed by the gap between the rings. The current in the loop is driven by an electromotive force, which is generated by applying a time varying electric field parallel to the axis of the ring shaped structure. The current generated follows a quasi-static model, where the current flows from one ring to another in the form of displacement current through the capacitance gap[37]. The magnetic current introduced by the QMC excites the bottom SSMPA through the coupling effect between devices via a coupling slot. As shown in Fig. 2(c), the proposed SSMPA element successfully excites the fundamental TM_{21} mode.

Next, this paper discusses the principles of bandwidth enhancement, as illustrated in Fig. 2. In the design, both the quarter-wavelength cavity (QMC) and the SSMPA are in an excited state. The QMC itself is capable of radiation, and this design expands the bandwidth through two different structures: one is to use the gap loading

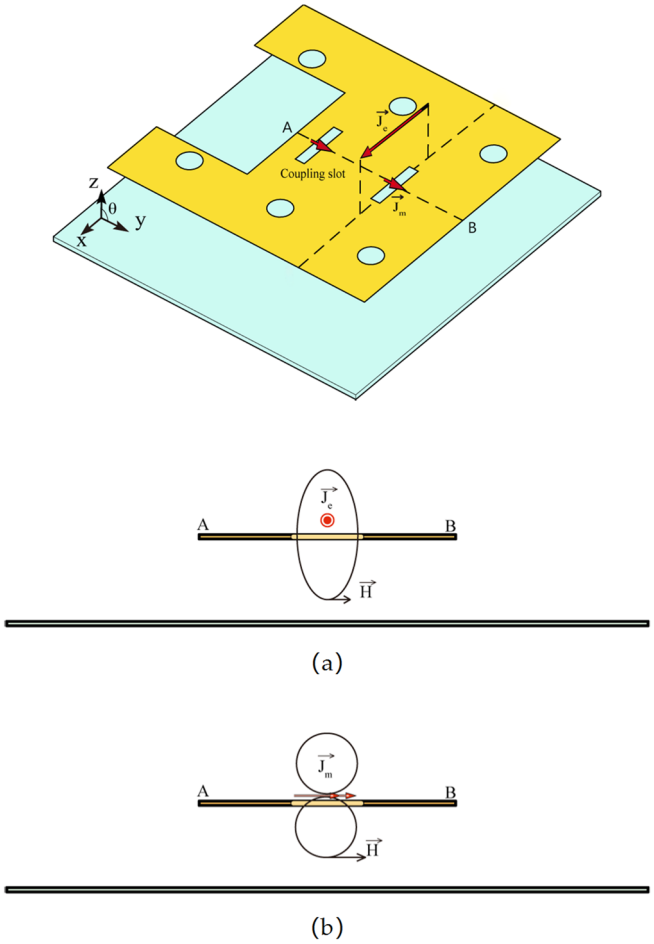

Fig. 1. Two types of excitation. (**a**) Electric current. (**b**) Magnetic-current excitation.

technique, and the other is to introduce a ring resonator. The larger the cross-sectional area of the guide ring, the greater the capacitance of the gap capacitor generated at the cutting point, and the smaller the resonance frequency. By keeping the width of the ring constant, increasing the spacing between the two rings decreases the capacitance between the rings, resulting in a significant increase in the resonance frequency. Without the inclusion of the ring resonator and slots, there is only one resonant point within the usable frequency band, as shown in Fig. 3(b). However, with the addition of the ring resonator, new resonant frequencies are introduced into the structure, thereby increasing the bandwidth and enhancing the practical usability of the design.

At the frequency of 4.7 GHz, due to the center-positioned coaxial feed used in the antenna array, the actual signal transmission path begins at the centrally located feed port and propagates along the transmission lines toward both sides. As shown in Fig. 4, distinct regions of varying radiation intensity can be clearly observed, which delineate the signal propagation paths and trends. Based on this information, the positions and design of the slots can be further optimized.

Series-fed sides-shorted MPA array

Magnetic current array

To implement a series array where each element is fed by magnetic current, a linear magnetic current array based on a microstrip structure (MS-MCA) was employed. The design of the microstrip transmission line was tailored to ensure linearity, resulting in the formation of the MCA. Using this approach, a three-element feed structure was designed on an F4BM substrate ($\varepsilon = 2.65$, $\tan\delta = 0.002$, $h_1 = 0.76$ mm), as shown in Fig. 3. This center-fed structure functions as a directional radiator, emitting electromagnetic waves. In the initial design phase, no ring resonator elements were included. The simulated $|S_{11}|$ parameters for the three rectangular patch antenna elements are shown in Fig. 2(b). The preliminary design of the MS-MCA achieved a narrow impedance bandwidth of 5.0–5.5 GHz (9.5%) with low return loss, providing a crucial foundation for subsequent design and optimization.

As described in Section II-B, by introducing ring resonators and constructing a dual-layer slot structure in the magnetic current-fed MPA array, two additional resonant points are introduced, forming new frequency bands. As shown in Fig. 5(b), the resonant point of the initial structure shifts, creating new resonant points on both sides. The right side resonant point is induced by the introduction of the ring resonator, while the left side resonant point arises from the addition of the slot structure. The resonant frequencies of these two elements

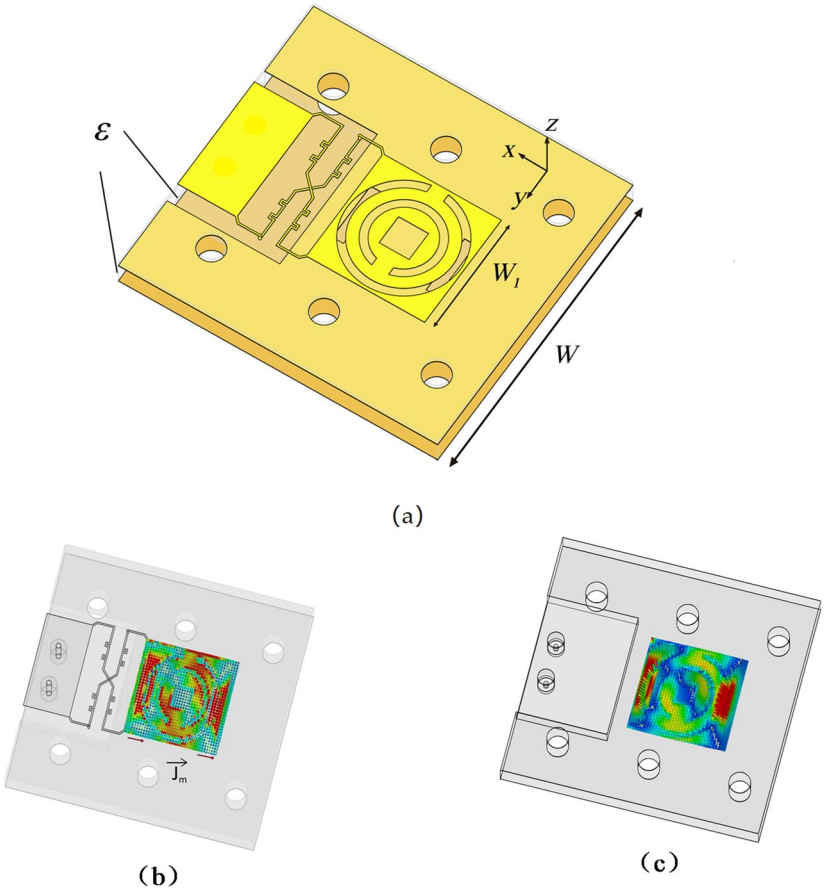

Fig. 2. Magnetic-current-fed MPA. (**a**) Element structure. E-field distribution of (**b**) QMC and (**c**) MPA at the operation frequency.

should be tuned to be close to the resonant frequency of the feed structure. The resonant frequency of the MPA elements can be adjusted by modifying the radius R of the ring resonator and the position and size L of the slot. The $|S_{11}|$ parameter curves for different R values are shown in Fig. 5(b) (c). As illustrated in the figure, with an increase in R_1 and R_2, the overall return loss curve shows a decreasing trend; as R_3 and R_4 increases, the return loss reaches a minimum at 4.7 GHz, satisfying the low VSWR requirement. The reason for choosing 4.7 GHz as the design frequency is twofold: on the one hand, 4.7 GHz optimizes the design of the antenna structure, not only to achieve the required broadband and low VSWR, but also to optimize the transmission path of the signal through the center-fed coaxial structure to reduce the impact of phase offset currents. It helps to improve the bandwidth, gain and impedance matching performance of the antenna, and ensures the stability and effectiveness of the antenna in the target frequency band. On the other hand, the 4.7 GHz frequency band is of great significance in practical applications, such as 5G base stations, unmanned aerial vehicles, and in vehicle communications, where it can achieve efficient data transmission and meet the needs of high speed and low latency applications. Therefore, the 4.7 GHz frequency is selected for this design, which not only improves the antenna performance at the technical level, but also closely connects with the actual application requirements. Considering the overall performance, the parameters were finally optimized to $R_1 = 8, R_2 = 10, R_3 = 13$ and $R_4 = 15$. The dimensions are shown in Table 1.

Antenna configuration

The MS-MCA feeds a series of MPAs through coupling slots to form a linear MPA array. The proposed MPA array structure is shown in Fig. 6. This antenna consists of two complete antenna structures stacked vertically, comprising a total of six layers. The figure clearly shows two closely stacked dielectric substrates, F1 and F2, with the feed positioned on the upper layer, F1. Four identical coupling slots are etched on the ground plane of the F1 layer and the top surface of the F2 layer. The MPA elements are located on the F2 layer of the F4BM substrate ($\varepsilon = 2.65$, $\tan\delta = 0.002$, $h_2 = 3.9$ mm). To achieve structural miniaturization, the feed network of the antenna array is designed in a curved shape to increase the edge to edge distance between adjacent patch elements, thereby further reducing the overall occupied space of the antenna.

During the design process, to avoid the overlap of transmission lines a and b, an air bridge structure was initially introduced. However, the final simulation results showed poor performance due to significant coupling effects between the two strips and the surrounding antenna patches, which disrupted the original electric field distribution of the antenna. To resolve the strong coupling issue caused by the close proximity of strips and

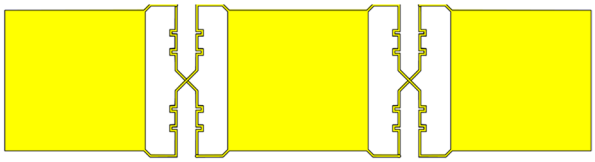

(a)

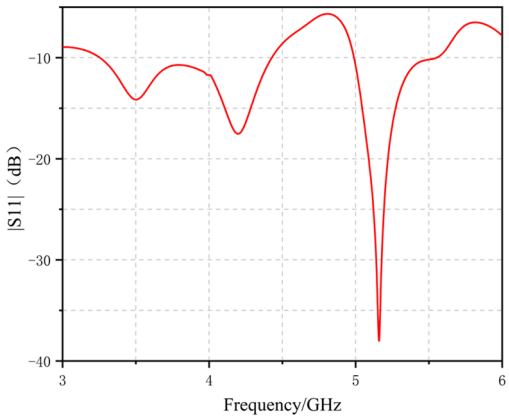

(b)

Fig. 3. (**a**) Initial MS-MCA structure diagram (**b**)S-parameter of the MS-MCA.

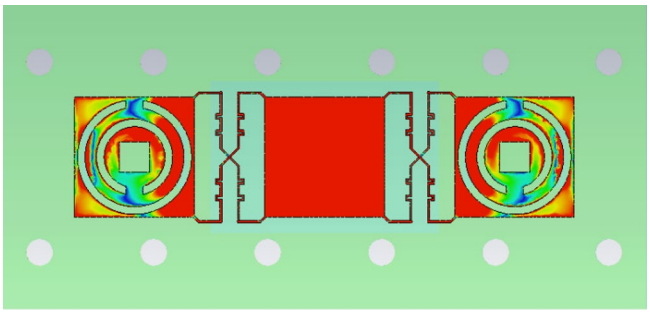

Fig. 4. Configuration of the proposed feeding structure and E-field distribution at 4.7 GHz.

patches, as shown in Fig. 5(a), the sections of the strips originally etched on the surface of F1 were moved to the backside of F1. Specifically, part of strip b was etched on the bottom layer of the lower substrate, and its near field coupling with the patches printed on the top layer of the upper substrate was shielded by a metal plane. The signal is conducted through metal vias in the middle, achieving electrical interconnection between the upper and lower layers.

It should be emphasized that, beyond size optimization, the design of the strips also takes into account the following considerations: Due to the loading effect of the strips, which disrupts the symmetry of the surface currents on the patch antenna relative to its diagonal, it is necessary to bend the strips to keep them as far away as possible from the square patch. However, excessive bending can increase the coupling between the two orthogonal strips, which may further degrade the orthogonality of the surface currents on the antenna. Therefore, the bending design of the strip structure aims to achieve an optimal balance between minimizing the impact on the patch elements and reducing the coupling effect between the two orthogonal strips. The dimensions are shown in Table 2.

In the design of the feed section, we adopted a center-fed configuration. The inner conductor of the SMA adapter passes through a hole at the center of the ground layer and is offset by a certain distance to achieve optimal slant-polarized impedance matching. Two rows of nylon standoffs are used to secure and support the upper dielectric substrate. Additionally, to ensure that the SMA adapter can connect from the back of the antenna to the microstrip line on the top F1 layer and achieve perfect matching, the diameter reserved for the RF line should be set according to the diameter of the SMA adapter's inner conductor. Soldering holes for the

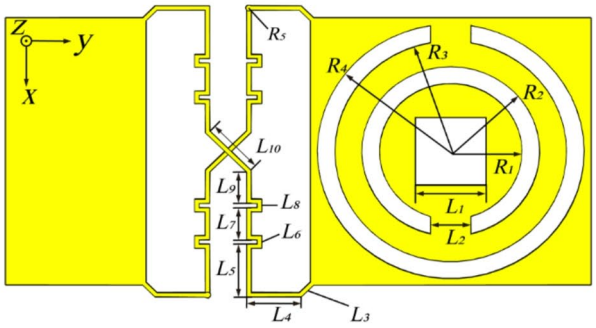

(a)

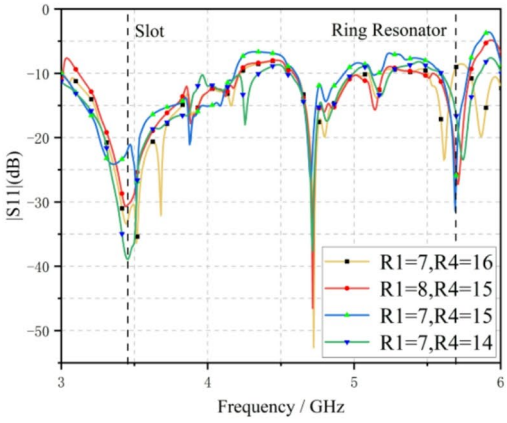

(b)

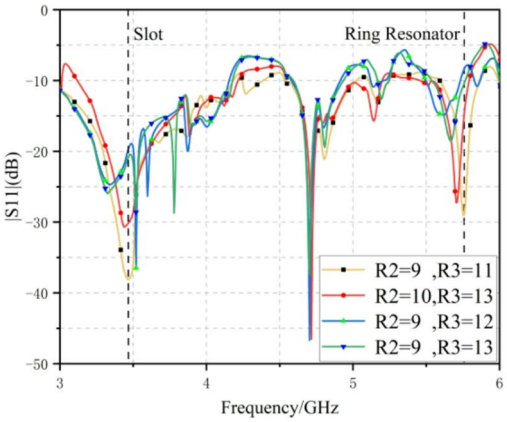

(c)

Fig. 5. (**a**) New MS-MCA structure diagram(**b**)(**c**) S-parameter of the MS-MCA.

top antenna elements also need to be pre-drilled. To achieve an ideal 50Ω impedance match, this design utilizes RG401-U coaxial cable[23].

The slot design for the metal slot layer and substrate F2 (as shown in Fig. 6(a-c)) is primarily intended to reduce the coupling effects between the metal strip b on the bottom of F1, the slot layer, and the SMA feed line. By incorporating this slot design, the distance between the feed line, the slot layer, and strip b is increased, thereby minimizing the impact of coupling effects on system performance.

R_1	R_2	R_3	R_4	R_5	L_1	L_2	L_3
8	10	13	15	0.36	8	4.5	2
L_4	L_5	L_6	L_7	L_8	L_9	L_{10}	
6.1	6.2	1.5	3.8	1.5	3.7	6.6	

Table 1. Dimensions of ant (Unit: mm).

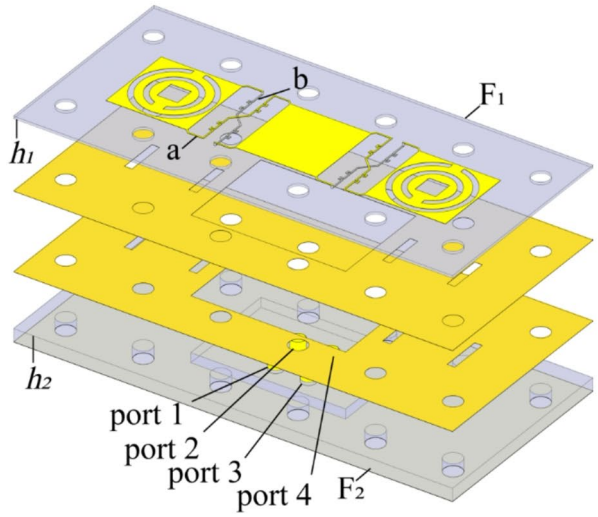

(a)

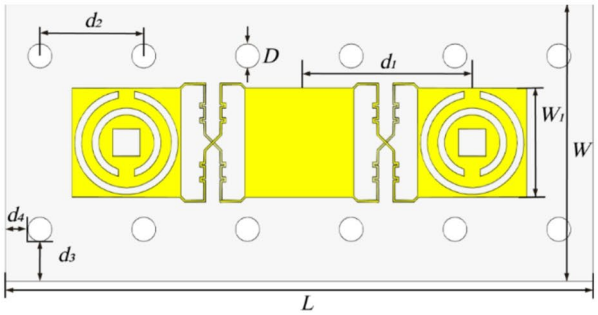

(b)

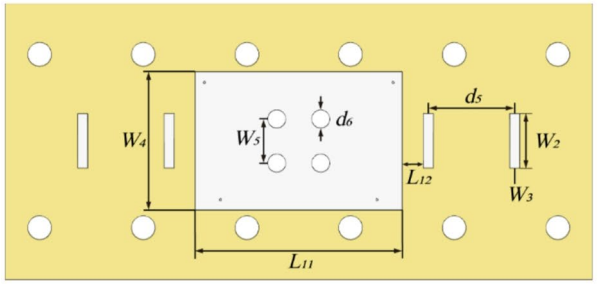

(c)

Fig. 6. Configuration of the proposed MPA array. (**a**) 3-Dview. (**b**)Top view. (**c**) Slot layer dimension diagram.

L	W	W_1	W_2	W_3	W_4	W_5	D
170	80	31.5	15.75	3	40	12.7	7
d_1	d_2	d_3	d_4	d_5	d_6	L_{11}	L_{12}
50	30	11.5	6.5	25	5.31	60	6

Table 2. Dimensions of ant (unit: mm).

Antenna analysis

The electric field radiation pattern of the antenna discussed in this paper was simulated using CST Microwave Studio, and the resulting images are shown below.

The electric field distribution of the proposed array at 4.7 GHz is shown in Fig. 7. The results indicate that the electromagnetic radiation of the MS-MCA is primarily concentrated in the central region, where the electric field intensity is stronger. The electromagnetic radiation of the MPA is mainly concentrated in the slot areas of the ring resonator and along the edges of the central slot. As illustrated in Fig. 7, the equivalent magnetic current along the x-axis is also demonstrated. The in phase current portion in the quarter-wavelength cavity (MCA) can be arranged along the y-axis. When fed from one port, the current on the strip is orthogonal to the current at the center of the patch surface; when fed from the opposite port, the overall current direction is reversed, maintaining orthogonal alignment. Compared to traditional series-fed microstrip patch antenna arrays, the two $\pm 45°$ feed ports in this design produce two mutually perpendicular slant-polarized radiations, thereby achieving dual polarization.

Implementation and measurement

To validate the proposed three-element linear array design, we fabricated a physical model and conducted measurements. The antenna array consists of two parts: an upper and a lower antenna section. During the manufacturing process, several fabrication issues needed to be considered, such as whether the selected feed line dimensions meet the processing requirements, how much soldering area should be reserved, whether the design structure conforms to the metal formation requirements of the PCB process, and the choice of the SMA feed line soldering position. Additionally, it was important to consider whether the addition of solder during the welding process would alter the electric field characteristics at relevant positions. In this design, the upper and lower layers were fabricated separately and then stacked together to form the desired structure. Twelve nylon screws were used to secure the two layers, minimizing the adverse effects of air gaps. A photo of the fabricated array is shown in Fig. 8.

The radiation performance of the antenna was measured using a far-field test system in an anechoic chamber. A comparison of the measured $|S_{11}|$ parameters and the simulated parameters is shown in Fig. 9(a). Under the criterion of $|S_{11}| < -10$ dB, the antenna achieved an ultra-wide bandwidth of 3 to 6 GHz (66%). Three similar resonant points can be observed in the figure, indicating good agreement between the test results and the simulation results. The shift in resonant frequencies is attributed to the introduction of screw holes, which disrupted the original surface wave transmission mode and affected the original resonant structure. The minor discrepancies between the test and simulation results may be due to fabrication errors.

Figure 9(c-h) show the isolation of the structure, where Fig. 9(g) shows that across the entire operational frequency band from 3 GHz to 6 GHz, the minimum value of the S*34* coupling measured between the two ports is -50dB, demonstrating good isolation. Figure 9(i) displays the gain of the structure, with test results indicating that the gain remains above 12.3 dBi throughout the entire operational bandwidth. Figure 9 (b) shows the standing ratio of the structure with a minimum of 1.007, suggesting that the overall structure exhibits excellent performance.

Figure 10 presents the radiation patterns at 3.5 GHz, 4.7 GHz, and 5.3 GHz. A good consistency between the measurement results and simulation results can be observed.

Finally, we compared the proposed array with previously reported series-fed arrays and dual-polarized antennas, and the results are summarized in Table 3. It can be seen that the antenna structure presented in this paper performs well in terms of maximum gain. Although the antenna described in reference[29] achieves a higher maximum gain, its design incorporates more radiating elements, leading to a more complex structure and significant coupling effects. In contrast, the antenna proposed in this paper utilizes a multilayer structure to achieve a satisfactory gain-to-area ratio.

Most high-gain patch antennas support only single polarization, whereas the antenna designed in this paper can achieve slant polarization. Moreover, the proposed antenna structure is a two-dimensional linear antenna array, which is significantly smaller in size compared to the previously reported dual-polarized antennas[17]. Building on this, by utilizing a dual-radiator structure, the antenna in this work demonstrates excellent performance in terms of gain and impedance bandwidth, achieving an ultra-wide bandwidth of 3 GHz and a minimum VSWR of 1.007, thereby extending the operational bandwidth. The comparison between this antenna array and other antenna arrays is shown in Table 3.

Conclusion

This paper proposes a 1×3 linear configuration series-fed slant-polarized MPA array using magnetic current feeding. Based on the classical series-fed antenna array, we have analyzed a dual-polarized array. In response to the current distribution within the antenna array, a modern miniaturization structural solution is proposed,

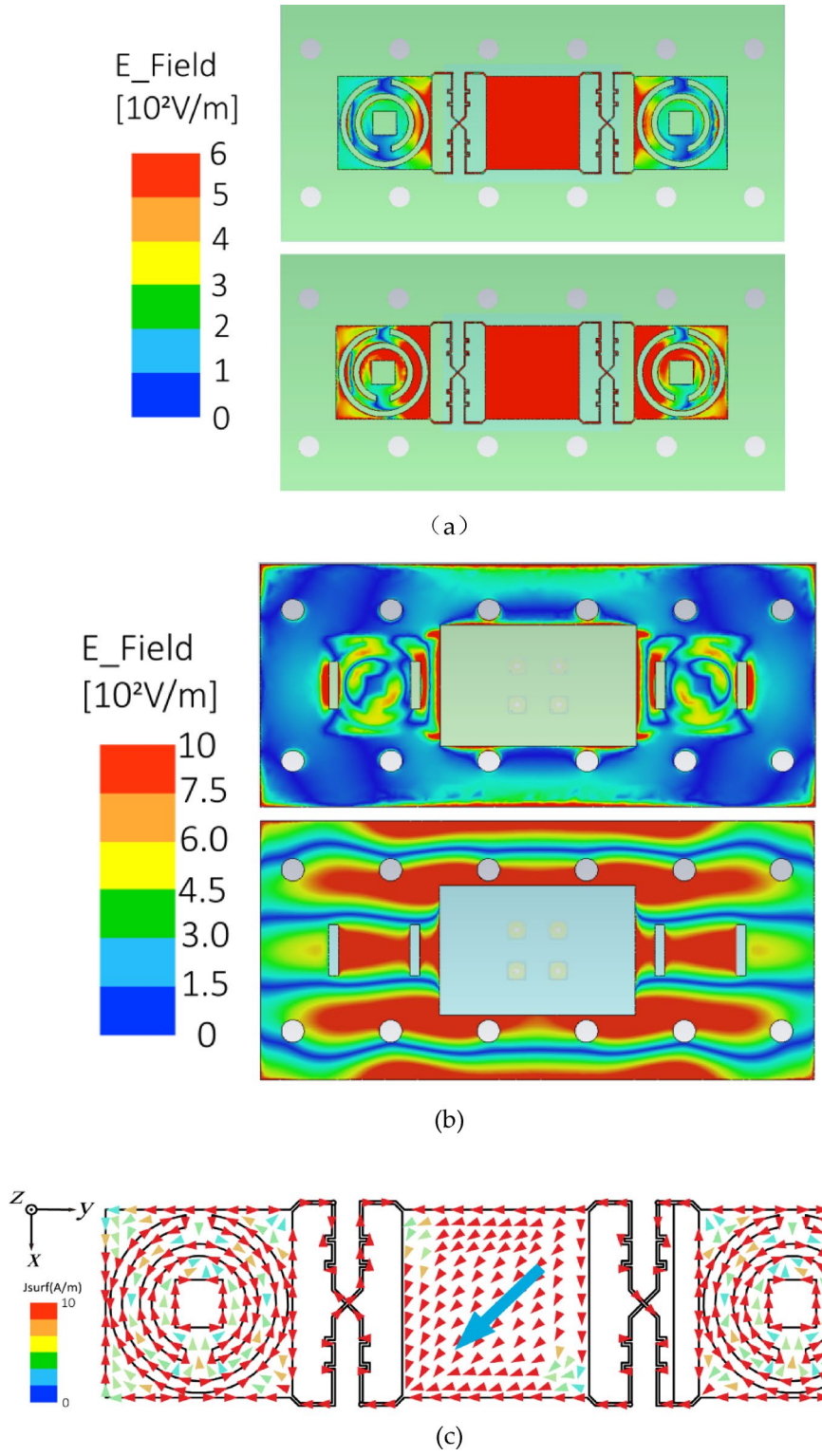

Fig. 7. E-field distribution at4.7 GHz (**a**) Feeding structure. (**b**) MPAs. (**c**) current distribution at 4.7 GHz.

effectively addressing the issue of large size in traditional dual-polarized antenna arrays. A prototype was fabricated and measured, validating the designed antenna's excellent performance in terms of low VSWR and ultra-wideband. The simulation results showed good agreement with the measured results. The proposed antenna demonstrates potential for high directivity and dual-polarization applications while providing a new practical method for bandwidth enhancement. This structure can be widely applied in various fields such as 5G communication systems, drones, radar systems, satellite communications, and IoT networks.

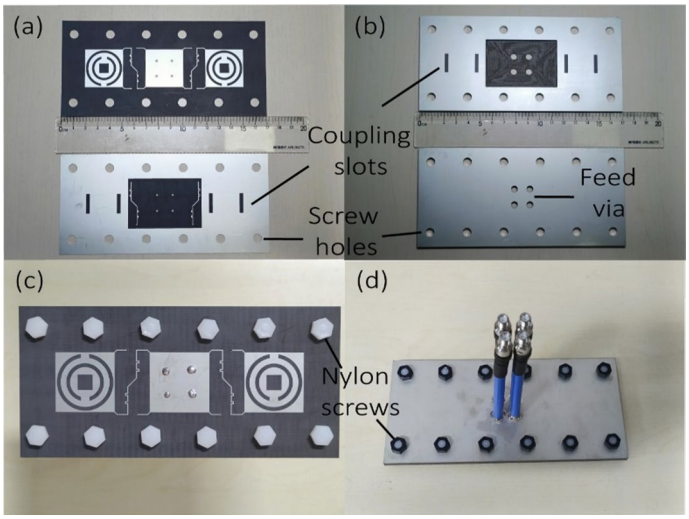

Fig. 8. Photos of the proposed array. (**a**) Unassembled layer-F1. (**b**) Unassembled layer-F2. (**c**) Front view of the assembled array. (**d**) Back view of the assembled array.

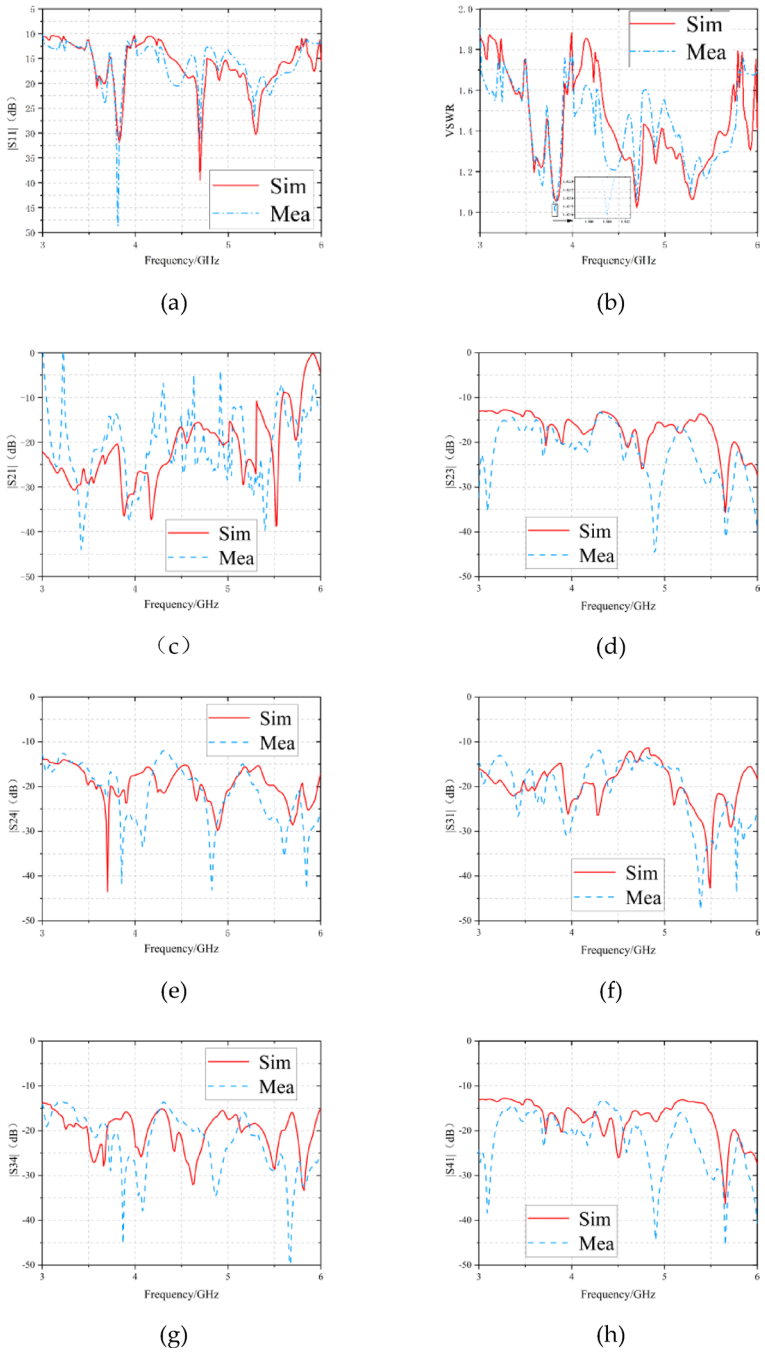

Fig. 9. (**a**) Reflection coefficient. (**b**) VSWR. (**c**-**h**) Isolation. (**i**) gain.

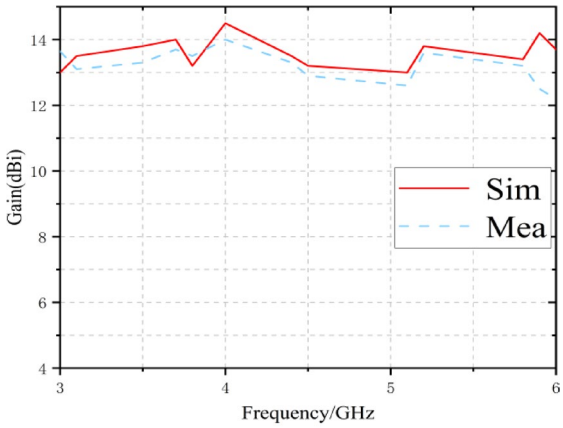

(i)

Fig. 9. (continued)

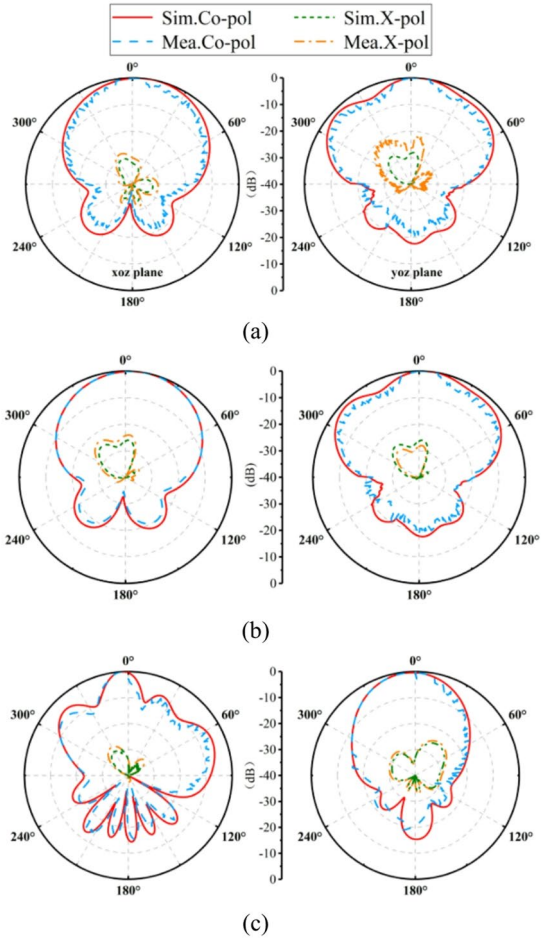

(a)

(b)

(c)

Fig. 10. Radiation patterns at (**a**) 3.8 GHz, (**b**) 4.7 GHz and (**c**)5.3 GHz.

Ref.	Frequency (GHz)	Polarization type	-10dB BW (%)	Profile (mm)	Array architecture	VSWR	Max gain (dB)
[9]	28.5	Slant DP	31.6	25 × 21	4 × 4	1.046	14
[17]	2.5	DP	14.34	240 × 20	1 × 8	1.094	6.01
[21]	4.9	SP	11.5	73 × 50	1 × 3	1.173	5.8
[22]	4.4	SP	41	150 × 75	1 × 8	1.094	5.8
[27]	5	SP	5.4	170 × 65	2 × 4	1.222	5.8
[29]	14	DP	7.8	79 × 79	2 × 8	1.119	18.4
[31]	10.5	SP	23.3	76 × 24	2 × 3	1.065	13.95
[32]	3.5	Slant DP	5.7	170 × 80	1 × 3	1.119	11.8
Prop.	4.5	Slant DP	66.7	170 × 80	1 × 3	1.007	14

Table 3. Comparisions of the relevant patch antennas. Abbreviations: Ref., reference; Prop., proposed; SP., single-polarized; DP., dual-polarized; BW., bandwidth.

Data availability

The data that support the findings of this study are available from the corresponding author upon reasonable request.

Received: 13 September 2024; Accepted: 17 November 2025
Published online: 22 January 2026

References

1. Li, M., Tian, S., Tang, M. C. & Zhu, L. Compact low-profile hybrid-mode patch antenna with intrinsically combined self-decoupling and filtering properties. *IEEETrans Antennas Propag.* **70** (2), 1511–1516. https://doi.org/10.1109/TAP.2021.3111638 (2022).
2. Chang, L. & Liu, H. Low-profile and miniaturized dual-band mi-crostrip patch antenna for 5G mobile terminals. *IEEE Trans. Antennas Propag.* **70** (3), 2328–2333. https://doi.org/10.1109/TAP.2021.3118730 (2022).
3. Crane, R. B. & Sharpe, C. B. Limitations of Series-Fed Arrays in Broadband Communications, in IEEE Transactions on Aerospace and Electronic Systems, vol. AES-2, no. 6, pp. 659–664, (1966). https://doi.org/10.1109/TAES.1966.4501959.
4. Yin, J., Wu, Q., Yu, C., Wang, H. & Hong, W. Low-sidelobe-level series-fed microstrip antenna array of unequal interelement spacing. *IEEE Antennas Wirel. Propag. Lett.* **16**, 1695–1698. https://doi.org/10.1109/LAWP.2017.2666427 (2017).
5. Chopra, R. & Kumar, G. Series-fed binomial microstrip arrays for extremely low sidelobe level. *IEEE Trans. Antennas Propag.* **67**, 4275–4279. https://doi.org/10.1109/TAP.2019.2908108 (2019).
6. Hamberger, G. F., Trummer, S., Siart, U. & Eibert, T. F. A planar dual-polarized microstrip 1-D-beamforming antenna array for the 24-GHz band. *IEEE Trans. Antennas Propag.* **65** (1), 142–149. https://doi.org/10.1109/TAP.2016.2618847 (2017).
7. Khalili, H., Mohammadpour-Aghdam, K., Alamdar, S. & Mohammad-Taheri, M. Low-cost series-fed microstrip antenna arrays with extremely low sidelobe levels. *IEEE Trans. Antennas Propag.* **66** (9), 4606–4612. https://doi.org/10.1109/TAP.2018.2845442 (2018).
8. Chen, F. C., Liang, Y. Z., Zeng, W. F. & Xiang, K. R. A Series-Fed Slant-Polarized microstrip patch antenna array. *IEEE Trans. Antennas Propag.* **72** (6), 5367–5372. https://doi.org/10.1109/TAP.2024.3394215 (2024).
9. Yun, S. J., Lee, K. H., Lee, J. N. & Cho, Y. K. An Inclined Bridge-Connected Magneto-Electric Dipole Array Antenna for Millimeter-Wave Broadband Applications. *IEEE Antennas Wirel. Propag. Lett.* **23** (7), 2140–2144 https://doi.org/10.1109/LAWP.2024.3382968 (2024).
10. Hoseini, M., Fooroghi, K. & Abdolali, A. A. Waveguide Slot-Fed Patch Antenna Array. IEEE Antennas Wirel. Propag. Lett. **22** (8), 2027–2031 (2023) https://doi.org/10.1109/LAWP.2023.3272151.
11. Yan, S. et al. A Wideband Gain-Enhanced Groove Gap Waveguide Slot Antenna Using Metal Pin Array. *IEEE Antennas Wirel. Propag. Lett.* **23** (1), 159–163 (2024). https://doi.org/10.1109/LAWP.2023.3320667
12. Zhang, Y., Li, H., Zhao, Y. & Li, Y. 2-D Epsilon-Near-Zero (ENZ) feeding network for High-Gain Millimeter-Wave slot antenna array using bulk silicon MEMS technology. *IEEE Trans. Antennas Propag.* **72** (4), 3055–3063. https://doi.org/10.1109/TAP.2024.3364749 (2024).
13. Yi, X. & Wong, H. Wideband Substrate Integrated Waveguide Fed Open Slot Antenna Array. *IEEE Access* **8**, 74167–74174 (2020). https://doi.org/10.1109/ACCESS.2020.2988053
14. Zhao, X. et al. Differentially-Fed slot array antenna backed with High-Order resonating cavity loading Slow-Wave Top–Bottom double pins. *IEEE Trans. Antennas Propag.* **72** (4), 3081–3091. https://doi.org/10.1109/TAP.2024.3363468 (2024).
15. Zha, L., Pan, Y. M. & Zheng, S. Y. Self-Decoupled linear and planar MIMO microstrip patch antenna arrays operating in the fundamental TM01 mode. *IEEE Trans. Antennas Propag.* **72** (2), 1224–1233. https://doi.org/10.1109/TAP.2023.3345409 (2024).
16. Jin, T. et al. Differentially fed Dual-Polarized antenna array using a structural composite Transmission-Line network. *IEEE Trans. Antennas Propag.* **72** (7), 6105–6110. https://doi.org/10.1109/TAP.2024.3404259 (2024).
17. Gao, Y., Ma, R., Wang, Y., Zhang, Q. & Parini, C. Stacked patch antenna with Dual-Polarization and low mutual coupling for massive MIMO. *IEEE Trans. Antennas Propag.* **64** (10), 4544–4549. https://doi.org/10.1109/TAP.2016.2593869 (2016).
18. Huang, W. et al. A Low-Profile Dual-Polarized Wideband Antenna for 5G Massive MIMO Base Station. *2021 IEEE International Workshop on Electromagnetics: Applications and Student Innovation Competition (IWEM), Guangzhou, China,* pp. 1–3 (2021). https://doi.org/10.1109/iWEM53379.2021.9790399
19. Lee, J. H. et al. Capacitively coupled microstrip comb-line array antennas for millimeter-wave applications. *IEEE Antennas Wirel. Propag. Lett.* **19** (8), 1336–1339. https://doi.org/10.1109/LAWP.2020.3001945 (2020).
20. Chang, L., Zhang, Z., Li, Y. & Iskander, M. F. Air sub-strate slot array based on channelized coplanar waveguide. *IEEE Antennas Wirel. Propag. Lett.* **16**, 892–895. https://doi.org/10.1109/LAWP.2016.2613965 (2017).
21. C.Tong, N., Yang, K. W., Leung & Liu, G. Design of MIMO antennas with DRAs and a Dual-Function Decoupling/Radiating monopole antenna. *IEEE Trans. Antennas Propag.* **72** (5), 3874–3885. https://doi.org/10.1109/TAP.2024.3378836 (2024).
22. Abubakar, S. H. et al. Eight element dual-band MIMO array antenna for modern fifth generation mobile phones. *AEUE - Int. J. Electron. Commun.* **175**, 155083. https://doi.org/10.1016/J.AEUE.2023.155083 (2024).
23. Wu, D. L., Chen,J. H., Yang, K. Y., Zhu, W. J. and Ye, L. H., A Compact Dual-Polarized Patch Antenna With L-Shaped Short Pins. *IEEE Antennas and Wireless Propaga. Lett.* **22**(4), 689-693 (2023)

24. Lv, D. et al. A Millimeter-Wave broadband Tri-Mode-Composite complementary source antenna array. *IEEE Trans. Antennas Propag.* **72** (7), 5733–5742. https://doi.org/10.1109/TAP.2024.3395895 (2024).
25. Chen, X., Han, L., Chen, X., Zeng, Q. & Zhang, W. A wideband coplanar waveguide antenna array with series feed. *IEEE Antennas Wirel. Propag. Lett.* **16**, 565–568 (2017). https://doi.org/10.1109/LAWP.2016.2590021
26. Mahdieh Ghaderi, P. & Rezaei Low profile wide band high gain transmitarray antenna for Ku band applications. *Opt. Commun.* **566**, 0030–4018. https://doi.org/10.1016/j.optcom.2024.130701 (2024).
27. Wu, S. T., Zhang, S. Q. & Wong, S. W. Compact broadband high directivity omnidirectional stripline antenna Array, in IEEE antennas and wireless propagation letters, https://doi.org/10.1109/LAWP.2024.3386806
28. Wu, L. X., Pan, Y. M. & Zheng, S. Y. Millimeter-Wave wideband Dual-Polarized Aperture-Coupled magnetoelectric dipole antenna array with high isolation. *IEEE Trans. Antennas Propag.* **72** (3), 2304–2313. https://doi.org/10.1109/TAP.2024.3352184 (2024).
29. Shukoor, M. A. et al. Design of miniaturized active matching network integrated ultrabroadband VHF/UHF monopole antenna for direction finding array Applications, in IEEE antennas and wireless propagation letters, **23**, 8, pp. 2436–2440, (2024). https://doi.org/10.1109/LAWP.2024.3394864
30. Zhu, L., Sun, J., Xu, G., Hao, Z. & Cao, Q. An integrated antenna array with Broadband, Low-RCS, and High-Gain characteristics. *IEEE Trans. Antennas Propag.* **72** (6), 5408–5413. https://doi.org/10.1109/TAP.2024.3396658 (2024).
31. Sun, D. M. et al. A planar UHF-Band ultrawideband modular antenna array with tapered probes feed. *IEEE Trans. Antennas Propag.* **72** (2), 1483–1496. https://doi.org/10.1109/TAP.2023.3348876 (2024).
32. Xu, H. et al. Wideband circularly polarized planar U-Shaped antenna array for Millimeter-Wave applications. *IEEE Trans. Antennas Propag.* **71** (8), 6971–6976. https://doi.org/10.1109/TAP.2023.3274948 (2023).
33. Chang, L., Zhang, Z., Li, Y. & Iskander, M. F. Single-layer magnetic current antenna array with high realized aperture usage rate based on microstrip line structure. *IEEE Trans. Antennas Propag.* **65** (2), 584–592. https://doi.org/10.1109/TAP.2016.2635622 (2017).
34. Chang, L., Li, Y., Zhang, Z. & Feng, Z. Horizontally polarized omnidirectional antenna array using cascaded cavities. *IEEE Trans. Antennas Propag.* **64** (12), 5454–5459. https://doi.org/10.1109/TAP.2016.2606555 (2016).
35. Chang, L., Zhang, Z., Li, Y. & Feng, Z. All-metal antenna array based on microstrip line structure. *IEEE Trans. Antennas Propag.* **64** (1), 351–355. https://doi.org/10.1109/TAP.2015.2500907 (2016).
36. Wang, B. et al. Wideband Series-Fed Microstrip Patch Antenna Array With Flat Gain Based on Magnetic Current Feeding Technology. *IEEE Antennas Wirel. Propag. Lett.* **22** (4), 834–838 (2023). https://doi.org/10.1109/LAWP.2022.3226461
37. Shalini, M. et al. Analysis of dual band emission in SRR integrated Terahertz photoconductive antenna. *Opt. Quant. Electron.* **55**, 101. https://doi.org/10.1007/s11082-022-04309-z (2023).

Acknowledgements

Thank you very much for the support of the School of Instrument and Intelligent Future Technology of North University of China.

Author contributions

Author Contributions: Conceptualization, Y.Z.; methodology, Y.Z.; software, Y.Z.; validation, X.J., and B.M.; formal analysis, Y.Z.; investigation, Y.Z.; resources, Y.Z.; data curation, Y.Z.; writing—original draft preparation, Y.J.; writing—review and editing, Y.Z and Y.Z; visualization, Y.S.; supervision, Q.W.; project administration, Q.W.; funding acquisition, M.L. All authors have read and agreed to the published version of the manuscript.

Funding

This research was funded by Double First-Class Talent Plan Construction(11012315); Double First-Class disciplines National first-class curriculum construction(11013168); Double First Class Disciplines Construction(11013351); National Future Technical College Construction Project(11013169).

Declarations

Competing interests

The authors declare no competing interests.

Additional information

Correspondence and requests for materials should be addressed to Q.W. or M.L.